Analysis of Vertical Fluorescence Resonance Energy Transfer from the Surface of a Small-Diameter Sphere

Gregory M. Jones,* Carla Wofsy,# Christina Aurell,§ and Larry A. Sklar*¶

Departments of *Pathology and #Mathematics and Statistics, The University of New Mexico, Albuquerque, New Mexico 87131, §College of Engineering, University of California, Riverside, California, and ¶Life Sciences Division, National Flow Cytometry Resource, Los Alamos National Laboratories, Los Alamos, New Mexico 87545 USA

ABSTRACT Fluorescence resonance energy transfer (FRET) measurements have been used to analyze fluorophore separations in a number of varying geometries, including small particles and extended surfaces. This study focuses on the geometry created by a donor extended above the surface of a small sphere (radius $< R_0$), where the acceptors are integrated into the sphere surface. The model of this geometry was based on an amphipathic molecule with its lipophilic region integrated into a detergent micelle and its hydrophilic region extending outward from the micelle surface, where the donor fluorophore is attached to the hydrophilic region of the molecule. Based on random acceptor incorporation into the micelle, a Poisson distribution was used to calculate the distribution of acceptor probes across the micelle population. The model converges to RET on a flat surface when the radius of the micelle exceeds $0.8\,R_0$. The model was also used to simulate FRET data showing that the positions of donors above the micelle surface could be uniquely resolved. Experimental verification of the model was achieved in a sulfobetaine palmitate micelle with fluorescein isothiocyanate donors attached to detergent-solubilized lipopolysaccharide (LPS) and lipophilic Fast-DiI acceptors. The use of steady-state analysis allowed resolution of cases in which donors were located at different distances from the surface. Combining steady-state with excited-state lifetime analysis allowed resolution of cases where there was a combination of distances. Given the large number of biomolecules that interact with lipids, this approach may prove generally useful for defining molecular conformation.

INTRODUCTION

Fluorescence resonance energy transfer (FRET) has been used in the study of many biological systems (Stryer, 1978; Matyus, 1992; Wu and Brand, 1994) with applications to liposome fusion (Chen and Knutson, 1988), molecular flexibility (Lakowicz et al., 1987; Maliwal et al., 1993), and macromolecular assembly both in solution and on cell surfaces (Sklar et al., 1980; Castanho and Prieto, 1992; Szabo et al., 1992). Due to the sensitivity of FRET to the distance of donor and acceptor separation, the geometry of the system has a significant influence on the analysis and interpretation of the measurements.

We have recently examined FRET between acceptors embedded in a micelle and donors associated with amphipathic molecules extending above the micelle surface (Aurell Wiström et al., 1996). Because of the general potential of such an approach for revealing details about molecular conformation, we have analyzed the system in more detail. Two classes of geometries are of interest with respect to this report: 1) FRET on the surface of a large sphere where the radius of the sphere is much larger than the Förster distance ($r \gg R_0$) and 2) FRET on the surface of small spheres where the radius of the sphere is smaller than the Förster distance ($r < R_0$). In the first case ($r \gg R_0$), which is representative of FRET on cell surfaces, the surface of the sphere may be approximated by a plane due to the relative insensitivity of FRET to the surface curvature (Fung and Stryer, 1978). This approximation allows each region on the sphere that contains a donor fluorophore to be treated as a separate entity, where the area of a region is defined by approximately $2.6\pi R_0^2$ (Estep and Thompson, 1979). As a result of this approximation, a homogeneous acceptor surface density (acceptors/cm^2 or acceptors/R_0^2) may be used to represent acceptor incorporation into the sphere population. In these cases, stoichiometric information regarding the acceptor-to-sphere ratio is not specifically considered (Fung and Stryer, 1978; Gibson and Loew, 1979; Wolber and Hudson, 1979; Doody et al., 1983; Kellerer and Blumen, 1984). As the diameter of the sphere and its surface area decreases, the distribution of acceptor chromophores across the sphere population is no longer homogeneous. Rather, a Poisson distribution describes the stoichiometry of acceptor incorporation for small proteins and micelles that bind acceptor chromophores randomly (Green, 1964; Gennis and Cantor, 1972; Kaschke et al., 1988). The Poisson distribution has been applied to tryptophan energy transfer in small proteins and the transfer between fluorophores on the micelle surface and in its interior (Green, 1964; Badley and Teale, 1971; Gennis et al., 1972; Sato et al., 1980; Ediger et al., 1983; Kaschke et al., 1988).

Received for publication 20 February 1998 and in final form 9 October 1998.

Address reprint requests to Dr. Larry A. Sklar, Cytometry, Cancer Center, R325, University of New Mexico Health Sciences Center, 2325 Camino de Salud, NE. Albuquerque, NM 87131-5636. Tel.: 505-272-4249; Fax: 505-272-6995; E-mail: lsklar@salud.unm.edu.

G. M. Jones is currently with the Center for Advanced Medical Technologies, Department of Radiology, University of Utah.

Supported by NIH grants GM37696 and RR01315 and the Cancer Research and Treatment Center, University of New Mexico Health Sciences Center.

0006-3495/99/01/517/11 $2.00

This report describes the analysis of energy transfer in a micelle system where donors can extend above the surface and where the sphere diameter is similar to the Förster distance. The approach is based upon a small diameter detergent micelle (~40 Å) with transfer between a donor covalently attached to an amphiphilic molecule solubilized in the micelle and acceptors partitioned into its surface. The random association of lipophilic acceptors with the micelle requires an explicit calculation of the distribution of the number of acceptors per micelle and the relative location of donors and acceptors.

MATERIALS AND METHODS

Materials

Fluorescein isothiocyanate (FITC) and 1,1-dilinoleyl-3,3,3′,3′-tetramethylindocarbocyanine, percholate (Fast-DiI) were purchased from Molecular Probes (Eugene, OR). Lipopolysaccharide (LPS) from the Re595 *S. minnesota* strain was a gift from Dr. Peter Tobias at The Scripps Research Institute (La Jolla, CA) or purchased from Sigma Chemical Co. (St. Louis, MO). Sulfobetaine palmitate (*N*-hexadecyl-*N*,*N*-dimethyl-3-ammonio-1-propane-sulfonate) (SBP), Trizma, NaCl, FITC-LPS from *S. ab. equi*, and wild-type *S. minn.* were all purchased from Sigma.

FITC labeling of LPS

LPS from *Salmonella minn.* Re595 was labeled with FITC using the method of Skelly et al. (1979). Labeling resulted in an approximate ratio of one FITC molecule per four to six LPS monomers. LPS content was determined using the malonaldehyde-thiobarbituric acid reaction (Cynkin and Ashwell, 1960). FITC concentration was calculated using absorption measurements from a Hitachi U-3210 spectrophotometer (Hitachi) and an extinction coefficient of 68,000 M^{-1} cm^{-1}.

Steady-state fluorescence measurements in micelles

The steady-state fluorescence was measured with an SLM Aminco 8000 spectrofluorimeter equipped with single grating excitation and emission monochromators (SLM Aminco, Rochester, NY) and a Hamamatsu R928-07 photomultiplier tube (Hamamatsu, Toyooka Vill, Japan). Excitation at 470 nm was used to minimize direct excitation of Fast-DiI (absorbance maximum, 549 nm). FITC-LPS concentrations were 30 nM in FITC and SBP was 100 μM. Using an aggregation number of 155, and a critical micelle concentration (CMC) of 15 μM with 85% of the detergent in micelles, gives a micelle concentration of 6×10^{-7} M (Herrmann, 1966; Aurell Wiström et al., 1996). The buffer consisted of 0.02 M Trizma, 0.15 M NaCl, pH 7.5. Data were corrected for inner and outer filter effects due to the varying Fast-DiI concentrations according to Shahrokh et al. (1991).

Excited-state lifetime measurements in micelles

Excited-state lifetimes of the donor were measured in an SLM 4850 multi-harmonic frequency spectrofluorometer (SLM Aminco) operated at 4–200 MHz. Excitation was from a 50-mW argon ion laser (Omnichrome, Chino, CA) at 488 nm. FITC-LPS was at a concentration of 300 ng/ml, based on LPS concentration. Fluorescence was detected through a Kopp 3-70 long-pass filter (Kopp, Pittsburgh, PA) combined with a 520-nm (10-nm full width at half-maximum bandpass) interference filter (Corion, Holliston, MA). Experiments were performed at 25°C in 1-cm quartz cuvettes. Excitation light scattered by oyster glycogen (Sigma) was used as a 0.0-ns reference. Analysis of the experimental data used a nonlinear least squares routine supplied by the manufacturer (SLM Aminco). The default values used as uncertainties in the measured phase angles and demodulation amplitudes were 0.5° and 0.5%, respectively.

Calculating the steady-state fluorescence as a function of the donor-to-micelle surface distance

If $p(t)$ is the probability that a donor, in the absence of acceptors, excited at $t = 0$ is still excited at time t, then the probability that a donor excited at $t = 0$ is still excited at time t in the presence of an acceptor, may be represented as (Wolber and Hudson, 1979):

$$p_a(t) = p(t)J(t) \tag{1}$$

The function p depends on τ, the mean excited-state lifetime of the donor, in the absence of acceptors:

$$p(t) = e^{-t/\tau} \tag{2}$$

and the factor J depends on τ, on the Förster distance R_0 for the particular donor and acceptor pair, and on the probability density function, $W(R)$, for the distance R between the donor and acceptor:

$$J(t) = \int_R e^{(-t/\tau)(R_0/R)^6} W(R)dR \tag{3}$$

In the case where there are k acceptors, each have the same probability density function W for its distance from the donor. If the locations of distinct acceptors are independent, then the probability that the donor, excited at $t = 0$, is still excited at time t is:

$$p_{a,k}(t) = p(t)[J(t)]^k \tag{4}$$

If energy transfer is viewed as taking place on a small micelle, the variable k represents the number of acceptors on the micelle surface. Thus, Eq. 4 holds for an individual donor isolated to a micelle containing k acceptors. Using the formalism of Wolber and Hudson (1979), the steady-state quantum yield of a donor isolated to a micelle that incorporates k acceptors is given by:

$$q_a = \frac{F_a}{F_0} = \frac{\int_0^\infty p_{a,k}(t)dt}{\int_0^\infty p(t)dt} \tag{5}$$

where F_a and F_0 are the donor steady-state fluorescence in the presence and absence of acceptors, respectively.

Equation 5 represents the steady-state quantum yield of a single donor in a micelle with k acceptors or a homogeneous population of donors in micelles with k acceptors. To better represent the situation where the micelle population is heterogeneous with regard to the number of acceptors, a Poisson distribution may be used to describe the micelle population (Ediger et al., 1984; Kaschke et al., 1988). The Poisson distribution is given by:

$$P(k) = \frac{e^{-L}L^k}{k!} \tag{6}$$

where $P(k)$ is the fraction of the overall micelle population with k acceptors and L is the ratio of acceptors to micelles. Fig. 1 shows the Poisson distribution for several values of L, the average acceptor-to-detergent micelle ratios. Note that at a mean ratio of 0.5 acceptors per micelle the majority (>60%) of micelles have no acceptors, whereas at a mean ratio of 1 acceptor per micelle the majority (>65%) of micelles incorporate one or more acceptors. We have also considered in Eqs. 21 and 22 (see Results) the case of a truncated Poisson that limits the total number of acceptors per micelle. Combining the Poisson distribution with Eq. 5 allows the descrip-

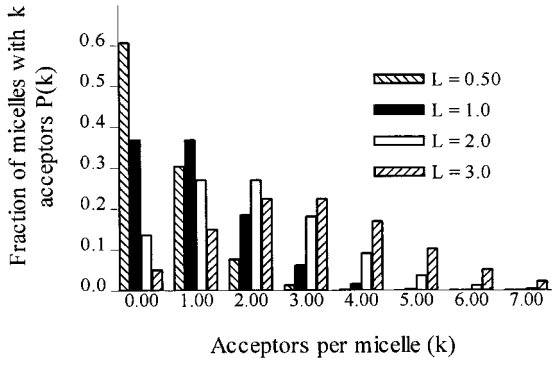

FIGURE 1 The Poisson distribution for various values of L (Fast-DiI to micelle ratios). Data are plotted as the fraction of micelles with k acceptors, $P(k)$, as a function of $L = 0.5$, 1.0, 2.0, and 3.0. This bar graph was produced using Eq. 6.

tion of F_a/F_0 as a function of the average acceptor-to-micelle ratio (i.e., $F_a/F_0 = f(L)$) (Green, 1964; Gennis and Cantor, 1972):

$$\frac{F_a}{F_0} = t^{-1}\int_0^{\infty} p(t)\sum_k^{\infty} P(k)[J(t)]^k dt$$

$$= t^{-1}\int_0^{\infty} p(t)\sum_k^{\infty}\left(\frac{e^{-L}L^k}{k!}\right)[J(t)]^k dt \qquad (7a)$$

using $\sum_0^k \frac{e^{-x}x^{-k}}{k!}(1-y)^k = e^{-xy}$ gives

$$= t^{-1}\int_0^{\infty} e^{-[(t/t)+L(1-J(t))]}dt$$

Inserting the substitution variable $u = t/\tau$ results in an expression for the quantum yield that is independent of τ.

$$\frac{F_a}{F_0} = \int_0^{\infty} e^{-[u+L(1-\bar{J}(u))]}du \qquad (7b)$$

where

$$\bar{J}(u) = \int_R e^{-u(R_0/R)^6}W(R)dR \qquad (7c)$$

The quantum yield q_a or, equivalently, the transfer efficiency $E = 1 - q_a$ is dependent on both the donor-acceptor separation (R) and the spectral properties of the donor-acceptor pair according to the Förster distance (R_0) given by:

$$R_0(\text{in angstroms}) = (Q_0 J\kappa^2 n^{-4})^{1/6}(9.79 \times 10^3) \qquad (8)$$

where Q_0 is the quantum yield of the donor in the absence of acceptors, n is the index of refraction of the medium separating the donor and acceptor, and κ^2 is the dipole-dipole orientation factor. The method of Dale et al. (1979), based on fluorescence polarization anisotropy measurements, was used to restrict the range of κ^2 (Aurell Wiström et al., 1996). The spectral overlap integral (J) was calculated for donor and acceptor pairs according to Aurell Wiström et al. (1996). As the transfer efficiency is sensitive to the separation of donor and acceptor where the distances are contained in the interval $0 \le R \le 2R_0$, and the micelle radius is $\sim 0.3R_0$, the micelle geometry needs to be taken into account (Ediger et al., 1984; Kaschke et al., 1988). An idealized model was built upon the extension of an amphipathic molecule (Fig. 2). If the position of the acceptor on the micelle surface is considered as an angular displacement relative to the donor, then the donor-acceptor separation (see Fig. 2) is given by:

$$R(D, \theta) = [(D + r)^2 + r^2 - 2(D + r)r\cos\theta]^{1/2} \qquad (9)$$

where D is the distance the donor is located above the micelle surface, r is the radius of the micelle, and θ is the angular displacement of the acceptor relative to the donor. With the micelle radius (r) and the donor to surface separation (D) constant, the probability distribution of R can be expressed as a function of θ. Expressions for quantum yield and energy transfer efficiency can be written in terms of a probability density for θ; i.e., $f(\theta) = \sin(\theta)/2$ for $0 \le \theta \le \pi$, where the probability of an acceptor being found in a region $2r^2 \sin\theta d\theta$ is calculated by integrating over θ and dividing this result by the total area of the sphere. For a small micelle with one acceptor, the efficiency of energy transfer is given by:

$$E = 1 - q_a = \int_0^{\pi} \frac{1}{1 + \left[\frac{R(\theta)}{R_0}\right]^6}\frac{1}{2}\sin(\theta)d\theta \qquad (10)$$

Integration, using the expression for $R(D, \theta)$ given by Eq. 9 results in the following expression for the transfer efficiency on a small-diameter micelle with a single acceptor:

$$E(D) = \frac{R_0^2}{4(D + r)r}\left[\frac{1}{6}\ln\left[\frac{(m + 1)^2}{m^2 - m + 1}\right] + \frac{1}{\sqrt{3}}\arctan\left(\frac{2m - 1}{\sqrt{3}}\right)\right]_a^b \qquad (11)$$

where the substitution variable $m = R^2(D, \theta)/R_0^2$, $a = (D/R_0)^2$, and $b = (r/R_0)^2$. For a population of micelles incorporating variable numbers of acceptors, the function $\bar{J}$ (Eq. 7c) needed to calculate the quantum yield (q_a) and transfer efficiency ($E = 1 - q_a$) has the form:

$$\bar{J}(u) = \int_0^{\pi} e^{-u(R_0/R(\theta))^6}\frac{1}{2}\sin(\theta)d\theta \qquad (12)$$

where R is given by Eq. 9, and the term (½) $\sin(\theta)d\theta$ is the result of using a probability density based on a spherical surface. The function can be used in this form to evaluate Eq. 7b numerically, or in the equivalent form:

$$\bar{J}(u) = \frac{u^{1/3}}{12(a + b)b}\int_{c_1}^{c_2} e^{-v}v^{-4/3}dv \qquad (13)$$

where $a = D/R_0$, $b = r/R_0$, $c_1 = ub^{-6}$, and $c_2 = u(a + b)^{-6}$. Equation 13 is derived from Eq. 12 through the use of the substitution variable $v = u(R_0/R(\theta))^6$. Integration by parts yields an expression that can be evaluated in terms of the gamma function $\Gamma(w)$, and the incomplete gamma function

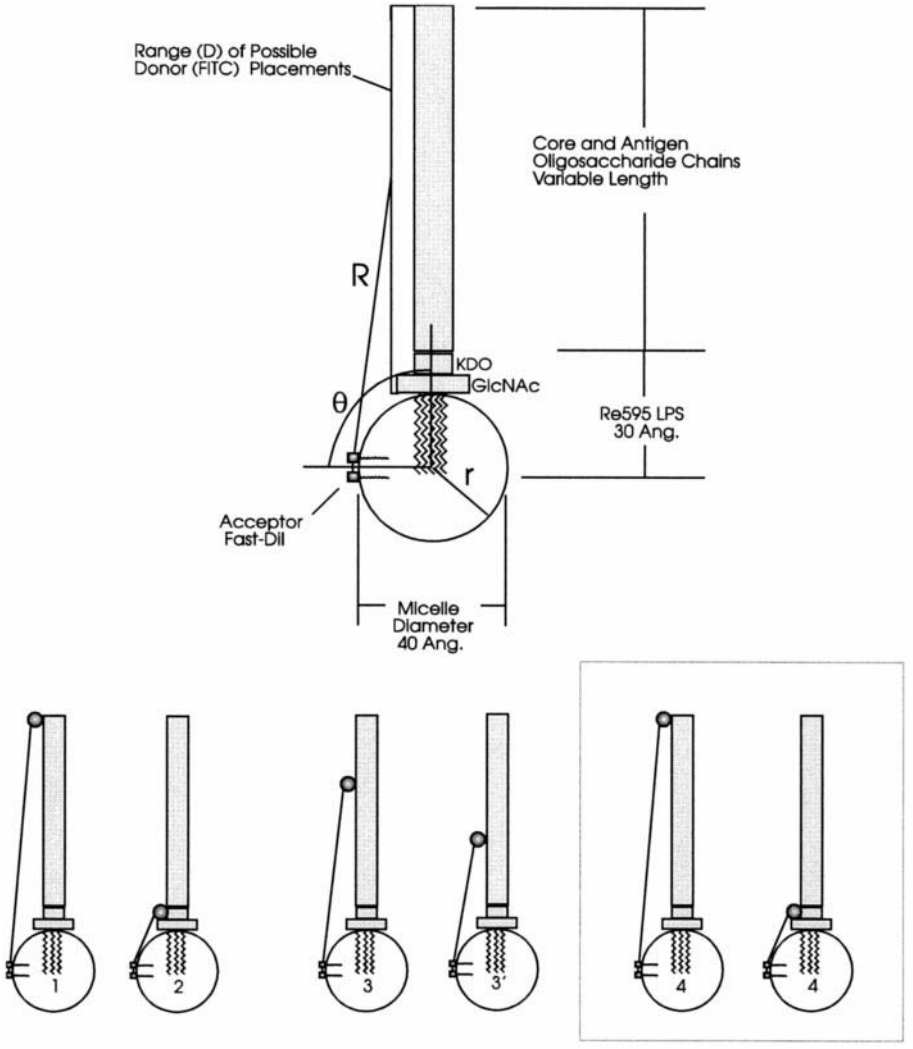

FIGURE 2 The micelle FRET model. R is the distance between the donor and the acceptor and can be calculated using Eq. 9. θ is the angular displacement along the micelle surface of the acceptor in relation to the donor. The amphipathic molecule is shown with its hydrophobic region integrated into the micelle and the hydrophilic region extended perpendicular to the micelle surface. The lower panel illustrates the cases examined in the steady-state and lifetime simulations. Case 1, $D = 1.8\ R_0$ (125 Å); case 2, $D = 0.01\ R_0$ (0.68 Å); case 3, $D = R_0$ (68 Å); case 3′, $D = 45$ Å; case 4, mixture of $D = 1.8\ R_0$ and $D = 0.01\ R_0$.

$\Gamma(w, x)$ (Abramowitz and Stegun, 1965):

$$\bar{J} = \frac{u^{1/3}}{4(a+b)b}\left(e^{-c_1}{c_1}^{-1/3} - e^{-c_2}{c_2}^{-1/3} - \Gamma(2/3) \cdot (\Gamma(2/3, c_1) - \Gamma(2/3, c_2))\right) \tag{14a}$$

$$\Gamma(w) = \int_0^\infty e^{-v} v^{w-1} dv \tag{14b}$$

$$\Gamma(w, x) = \int_x^\infty e^{-v} v^{w-1} dv \tag{14c}$$

Simulation of the excited-state lifetime data

As FRET is a dynamic process, the decrease in the excited-state lifetime of a quenched donor is proportional to the decrease in fluorescence (Lakowicz, 1983), as:

$$\tau = \tau_0\left(\frac{F_a}{F_0}\right) \tag{15}$$

where τ_0 is the unquenched excited-state lifetime of the donor. Because the overall fluorescence is due to emission from both quenched and nonquenched donors the total excited-state lifetime decay in the micelle system is best represented as a sum of individual exponential decays:

$$I(t) = \sum_n \alpha_n e^{-t/\tau_n} \tag{16}$$

where τ_n is the lifetime of the individual component, which may be an unquenched donor or donors variably quenched with an efficiency according to Eq. 10, and α_n is the associated pre-exponential term. The fractional contribution of the total fluorescence by the population of donors whose lifetime is τ_n, is given by:

$$f_n = \frac{\alpha_n \tau_n}{\sum_k \alpha_k \tau_k} \tag{17}$$

The quantities α_n and f_n are dependent upon the acceptor distribution in the micelle population (i.e., the Poisson distribution).

Simulation of the steady-state FRET data

Steady-state fluorescence data were simulated using Eq. 7b, with $\bar{J}$ substituted from Eq. 13. For a LPS molecule with one donor at distance D and

a micelle with multiple acceptors on its surface, the quantum yield is a function of $\bar{J}$ and D:

$$q_a(D) = \frac{F_a}{F_0}(D) = \int_0^\infty e^{-[u+L(1-\bar{J}(u)]}du \qquad (18)$$

To represent LPS molecules with two possible donor labeling sites (D_1, D_2):

$$\frac{F_a}{F_0}(D_1, D_2) = Aq_a(D_1) + (1 - A)q_a(D_2) \qquad (19)$$

Equations 18 and 19 were used to evaluate the geometrical cases shown in Fig. 2.

Simulation of lifetimes in the FRET system

Transfer efficiencies were simulated using Eq. 11 and translated into lifetimes through Eq. 15. To compare the lifetime models with the actual measurements, the modeled lifetime data were transposed from values of α and τ to phase and modulation values (Eis and Lakowicz, 1993).

Fitting of steady-state FRET data in the micelles

Fitting of the steady-state data was done using Eqs. 18 and 19. Statistical analysis was limited to the calculation of the standard deviation (σ) using the formula:

$$\sigma = \left[\frac{\sum_j (Y_{calj} - Y_{obsj})^2}{DOF}\right]^{1/2} \qquad (20)$$

where Y_{calj} is the jth calculated value, Y_{obsj} is the jth experimentally observed value, and DOF reflects the degrees of freedom used in the fit. Degrees of freedom was calculated by subtracting the number of fit parameters from the number of data points being fit. Fits using Eq. 18 were calculated with one fit parameter (D), whereas fits using Eq. 19 were done with three fit parameters (D_1, D_2, and A). Unless otherwise stated, data fitting, simulations, and statistical analysis were performed using The Scientist software package (Micromath, Salt Lake City, UT) and MATLAB (The Mathworks, Natick, MA).

RESULTS

Steady-state FRET quenching simulations

To examine the ability of FRET to resolve donor positioning above the sphere surface, several cases were simulated using Eq. 19 (Figs. 2 and 3 and Table 1). Two parameters were varied: 1) the distance of donor placement (D) from the surface of the sphere and 2) the proportion of donors at short, intermediate, or large separations from the sphere surface (Fig. 2). The cases examined were 1) 100% extended donor attachment (125 Å, $D > 1.5\ R_0$), 2) 100% near the sphere surface donor attachment (0.68 Å, $D \ll R_0$), 3) 100% intermediate distance (68 Å ($D \approx R_0$) and 45 Å), and 4) a population consisting of a 1:1 ratio ($A = 0.5$) of extended and near donor locations. As observed in Fig. 3, donors at different distances are distinguished by the magnitude of energy transfer whereas the heterogeneous placement of donors is distinguished in the dependence of transfer on the acceptor density. Note the comparison of case 4 to case 3 (45 Å), where the transfer is similar at one acceptor per micelle.

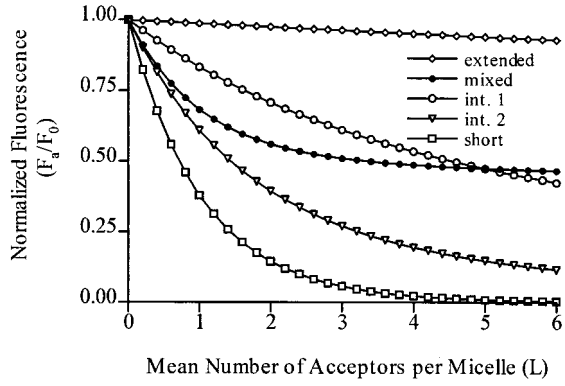

FIGURE 3 Calculated steady-state fluorescence in the micelle FRET model. Plots show F_a/F_0 versus L for the geometries of Fig. 2. Case 1 (◇), all donors are extended (D = 125 Å) 1.8 R_0 away from the micelle surface; case 2 (□), all donors are extended (D = 0.68 Å) 0.01 R_0 away from the micelle surface; case 3 (○), all donors are extended (D = 68 Å) R_0 away from the micelle surface; case 3′ (▽), all donors are extended 45 Å away from the micelle surface; case 4 (●), 50% of the donors are extended (D_1) 0.01 R_0 and 50% are extended (D_2) 1.8 R_0 away from the micelle surface.

Excited-state lifetime simulations

Donor excited-state lifetimes were simulated (Fig. 4) using Eq. 15 and translated into phase and modulation data (Table 2) (Eis and Lakowicz, 1993). A lifetime of 3.98 ns was used to mimic native FITC. Single-component, dual-component, and distributed lifetimes (not shown) were considered. When all donors were extended away from the micelle surface (case 1), a single near native lifetime produced an adequate fit, with a range of 3.93–3.76 ns for donor-to-micelle ratios (L) of 1–5, respectively. When all donors were located near the micelle surface (case 2), the near native lifetime component was a result of unquenched donors resident on spheres that contain no acceptors, whereas the shorter lifetime corresponds to donors quenched by a sphere resident acceptor or acceptors. As would be expected, the fraction (see Eq. 17) of signal from the near native lifetime decreased with increasing acceptor-to-micelle ratio. Using a single component fit, quenching of donors at intermediate distances (case 3) exhibited lifetimes that ranged from 3.31 to 1.69 ns, corresponding with acceptor-to-micelle (L) from 1–5. The range of lifetimes in case 3 results in part from transfer efficiencies (E) that vary from 0.06 to 0.50, depending upon the relative location of donor and acceptor on the micelle compared with R_0. Mixtures of donors (case 4) were accommodated with two distinct lifetimes: the near native and the near 0-ns lifetime. In contrast to case 1, the fraction of intensity from the long lifetime in case 4 increased with increasing L, which was expected as a portion of the donors were well extended from the surface of the micelle. Fig. 4 shows clear resolution between cases

TABLE 1 Summary of micelle FRET for various geometries

Case	% large D	% intermediate D	% small D	$E(D_1)$	$E(D_2)$	A
1	100	0	0	0.02		1.00
2	0	0	100	0.99		1.00
3	0	100 (68 Å)	0	0.18		1.00
3′	0	100 (45 Å)	0	0.53		1.00
4	50	0	50	0.99	0.02	0.50

Five cases are shown: 1) exclusively large D (125 Å); 2) exclusively small D (0.68 Å); 3) exclusively intermediate D (R_0, 68 Å); 3′) exclusively intermediate D (45 Å); 4) a heterogeneous mixture (1:1) of small (0.01 R_0, 0.68 Å) and large (1.8 R_0, 125 Å) donor to micelle surface distances.

3 (45 Å) and 4 for one acceptor per micelle, which is not resolved in the steady-state analysis.

Effects of Förster distance (R_0) and acceptors per micelle (k) on transfer

Energy transfer is dependent upon the ratio of R_0 and the micelle radius (Fig. 5 *A*). For a constant micelle radius, the accessible distances vary according to R, suggesting that R_0 for a donor-acceptor pair can be used to select the sensitivity of transfer to different distances as is the case for FRET in other geometries. The case of multiple acceptors per small sphere ($k > 1$) was also examined (Fig. 5 *B*). The donor quantum yield was approximated from Eq. 5 by the relationship $q_a = R^6/(R^6 + k)$, where R was expressed as a multiple of R_0. The effect of 10 acceptors was to increase the effective R_0 by ~50%.

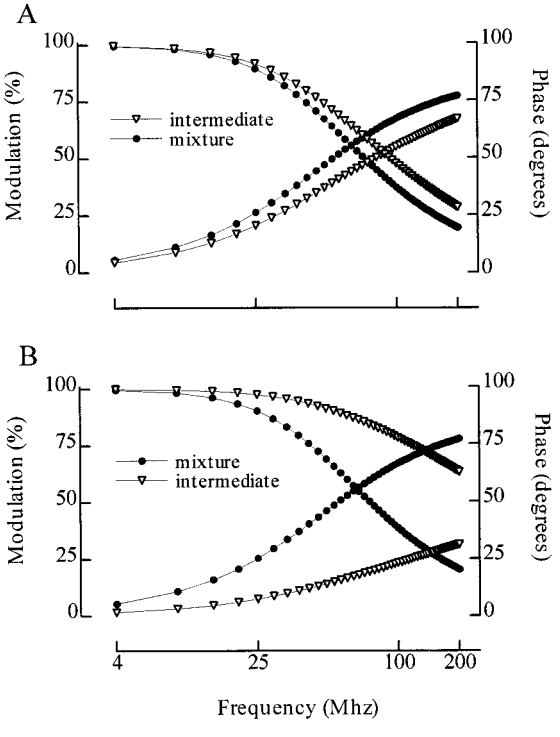

FIGURE 4 Simulated fluorescence lifetime data in the micelle FRET model. (*A*) Phase and modulation calculated at $L = 1.0$. Case 3′ (△), a homogeneous donor-to-micelle surface separation of intermediate size (45 Å); case 4 (●), a 1:1 mixture of donors 1.8 R_0 (125 Å) and 0.01 R_0 (0.68 Å) from the micelle surface. (*B*) Phase and modulation calculated at $L = 5.0$. Case 3′ (△); case 4 (●). From Eq. 6, at $L = 1$, $P(0) = 0.368$, and at $L = 5$, $P(0) = 0.006$.

Analysis of transfer in the model micelle system

We measured quenching of FITC-labeled *S. minn.* Re595 LPS, *S. ab. equi* LPS, and *S. minn.* LPS by Fast-DiI solubilized in SBP as previously described (Aurell Wiström et al., 1996). The potential fluorophore linkage sites are the phosphoethandamine (PEtn), 4-amino-4-deoxy-L-arabinose (AraN), core polysaccharide, and *O*-antigen polysaccharide regions (Fig. 6). As shown in Fig. 7, the quenching efficiency, as a function of acceptor concentration, of Re595 FITC-LPS was substantially higher relative to the *S. minn.* FITC-LPS, whereas FITC-LPS from *S. ab. equi* exhibited an intermediate quenching efficiency. These results correlated with the extension of the various oligosaccharide chains of LPS from the micelle surface, where *S. minn.* LPS was extended well away from the micelle surface and *S. minn.* Re595 LPS was near the surface, whereas *S. ab. equi* LPS exhibited an intermediate oligosaccharide extension (Kastowsky et al., 1992; Aurell Wiström et al., 1996).

We analyzed these experiments (Fig. 7 and Table 3) using Eq. 18, allowing transfer at a single donor-to-micelle separation (D), and Eq. 19, allowing for transfer at two discrete distances, D_1 and D_2. The single-component fit to the data from *S. minn.* Re595 FITC-LPS produced a range of donor-to-surface separation (D) of ~16–36 Å, whereas the single-component fit to the *S. ab. equi* data produced a donor-to-surface separation of 38–56 Å. The single-component fit for *S. minn.* wild-type data produced a FITC-surface separation of 67–91 Å. Distance ranges are given to reflect uncertainties in κ^2, the dipole-dipole orientation factor (Dale et al., 1979). To calculate the dipole-dipole orientation factor, fluorophore motion was estimated using fluorescence anisotropy measurements (Aurell Wiström et al., 1996). Anisotropy values were translated into variances of κ^2 using the method of Dale et al., 1979.

When the wild-type *S. minn.* data were fit by Eq. 19, ranges for D_1 and D_2 were found to be 34–51 Å and 92–122 Å with 77% of the intensity coming from the larger distance. The fit to *S. ab. equi* data yielded donor-to-surface separations of 11–25 Å and >150 Å with 27% at the longer distance. The analysis does not distinguish further heterogeneity in FITC attachment sites or chain lengths. Although

TABLE 2 Model and fit parameters

Model Parameters				Fit Parameters					
D_1 (Å)	D_2 (Å)	A	DiI/micelle	τ (ns)	χ^2	τ_1 (ns)	τ_2 (ns)	α_1	χ^2
1.25		1.0	1	3.93	1.9×10^{-3}	3.96	3.85	0.77	1.9×10^{-7}
			2	3.79	4.0×10^{-3}	3.94	3.76	0.65	3.3×10^{-7}
			3	3.77	4.8×10^{-3}	3.92	3.77	0.49	2.7×10^{-7}
			4	3.76	4.1×10^{-3}	3.84	3.76	0.33	1.7×10^{-7}
			5	3.76	2.8×10^{-3}	3.90	3.76	0.20	0.9×10^{-7}
0.68		1.0	1	3.89	0.61	3.98	0.04	0.50	2.3×10^{-6}
			2	3.80	1.22	3.98	0.04	0.32	8.5×10^{-6}
			3	3.71	1.82	3.98	0.04	0.24	1.8×10^{-5}
			4	3.62	2.42	3.98	0.04	0.19	3.2×10^{-5}
			5	3.53	3.00	3.98	0.04	0.16	5.1×10^{-5}
68		1.0	1	3.31	0.54	3.69	2.28	0.70	0.01
			2	2.75	1.14	3.32	1.75	0.60	0.03
			3	2.29	2.29	3.05	1.52	0.44	0.04
			4	1.94	1.94	2.87	1.43	0.30	0.03
			5	1.69	1.38	2.74	1.38	0.18	0.02
45		1.0	1	2.72	3.11	3.67	1.17	0.51	0.18
			2	1.97	5.08	3.19	0.83	0.43	0.41
			3	1.48	6.27	2.75	0.61	0.23	0.58
			4	1.03	7.12	2.35	0.44	0.16	0.66
			5	0.84	7.73	2.02	0.30	0.10	0.61
0.68	125	0.5	1	3.92	0.17	3.95	0.05	0.80	5.9×10^{-5}
			2	3.88	0.15	3.90	0.06	0.84	2.7×10^{-3}
			3	3.84	0.09	3.85	0.07	0.92	3.3×10^{-3}
			4	3.81	0.05	3.81	0.10	0.97	2.7×10^{-3}
			5	3.79	0.02	3.79	0.12	0.99	1.8×10^{-3}

Cases analyzed are as in Fig. 2 and Table 1. Acceptor concentration results in a ratio of 1, 2, 3, 4, and 5 acceptors per micelle. Using Eq. 6 produces values for $P(0)$ of 0.368, 0.135, 0.018, and 0.006, respectively. One (τ) and two (τ_1, τ_2) lifetime component fits are shown with the pre-exponential coefficient (α_1) of τ_1 and the goodness-of-fit (χ^2). Calculations for this table used a value of 68 Å for R_0.

the *S. minn.* Re595 LPS presents donors only near the micelle surface, the placement of 9% of the donors at a large distance in the two-component fit may represent experimental uncertainty. In this system, uncertainty comes from the true ratio of acceptors incorporated into micelles (based on acceptor concentration and CMC) or errors in fluorescence transfer measurements due to inner or outer filter corrections. Alternatively, the deviation may be due to the assumption that the micelle offers an unlimited acceptor binding capacity, as in Eq. 7. A truncated Poisson distribution (Haight, 1967), for example, places a limit (N) on the number of acceptors that can be incorporated into a single micelle. The truncated Poisson distribution (P_T) is represented by:

$$P_T(k) = \frac{e^{-L} L^k \Gamma(N+1)}{k!\Gamma(N+1, L)} \quad k = 0, 1, \ldots N, \tag{21}$$

where $\Gamma(N + 1)$ and $\Gamma(N + 1, L)$ denote the gamma function and the incomplete gamma function, (Eq. 14b,c). Equation 7b for the quantum yield changes accordingly:

$$\frac{F_a}{F_0} = \int_0^\infty e^{-u} \sum_{k=0}^{N} P_T(k)[\bar{J}(u)]^k dt \tag{22}$$

The function $\bar{J}$ (Eq. 7c) is unchanged. The data are fit with a single component when N is ~4 (data not shown).

Excited-state lifetime analysis in the model system

Table 4 summarizes the lifetime measurements on the three FITC-LPS preparations with 0, 1, and 2 Fast-DiI acceptors per micelle. In all cases, with or without Fast-DiI, the fluorescent signal was dominated by the naive lifetime (>3.7 ns) of fluorescein. This corresponds to simulated lifetime data, in cases where the native lifetime dominated (see Table 2). In contrast, quenching of donors placed wholly at an intermediate distance ($D \approx R_0$) would exhibit an intermediate lifetime (case 3).

All of the experiments are complicated by the presence of short lifetimes, even in the absence of the acceptor, of unknown origin but possibly related to residual FITC-FITC or FITC-LPS interaction. The presence of the acceptor, Fast-DiI, increases the fraction of the short-lifetime species and a loss of long-lifetime species. As would be expected, the α_2/α_1 values are higher for the Re595 mutant when compared with either *S. ab. equi* or *S. minn.* wild type. This is in agreement with the model in which the entire donor population of Re595 is near the surface of the micelle, whereas *S. ab. equi* and *S. minn.* consist of donors both near and extended away from the surface.

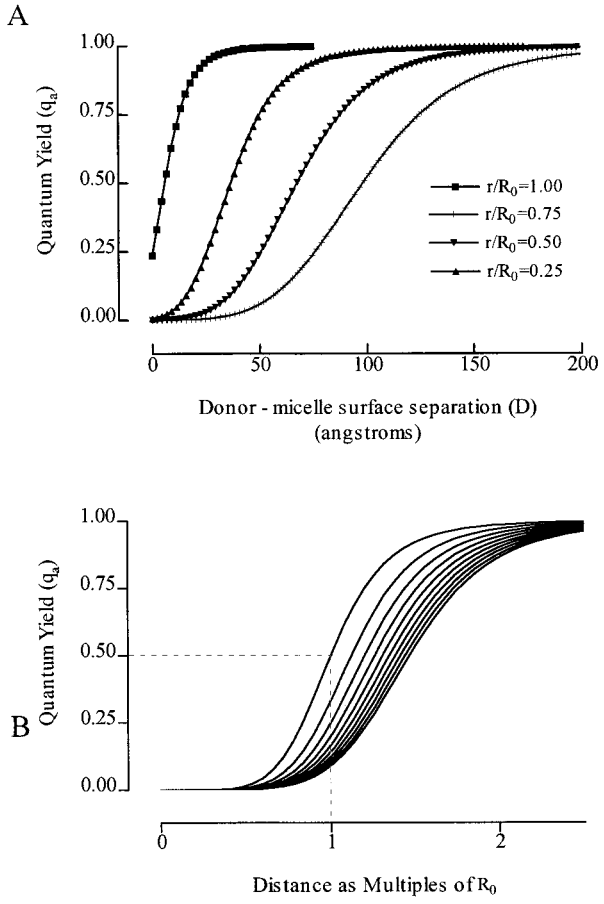

FIGURE 5 (*A*) Quantum yield (q_a) as a function of R_0 and D. Data were generated using Eq. 11 for four ratios of r/R_0, where the distance of separation (D) between the donor and the micelle surface is varied from D = 0.1 Å to 200 Å. ■, r/R_0 = 1.0; ▲, r/R_0 = 0.75; ▼, r/R_0 = 0.50; +, r/R_0 = 0.25. (*B*) Quantum yield (q_a) as a function of the ratio R/R_0 in the presence of k acceptors, a fixed distance R from the donor. R_0 denotes the Förster distance. When R is fixed, Eq. 3 of Estep and Thompson (1979) holds and reduces to $q_a = F_k/F_0 = 1/(1 + k((R_0/R)^6)) = (R/R_0)^6/(k + (R/R_0)^6)$. The same result is obtained by taking R constant in the equation for $J(t)$ in this paper. From Eq. 3, i.e., $J(t) = \exp[(-t/\tau)(R_0/R)^6)]$. Then Eq. 4 becomes $P_{a,k}(t) = \exp[(-t/\tau)(1 + k(R_0/R)^6)]$ and the expression for q_a follows from Eq. 5. The value of k ranges from 1 to 10 in increments of 1 (left to right), fluorophore separation (R) is presented as multiples of the Förster distance (R_0).

DISCUSSION

FRET has been studied for geometries ranging from acceptors extended above a small protein that incorporates donor fluorophores to transfer on large infinite sheets (Badley and Teale, 1971; Fung and Stryer, 1978; Wolber and Hudson, 1979; Sklar et al., 1980) as well as in or on detergent micelles (Sato et al., 1980; Ediger et al., 1983; Kaschke et al., 1988). This report describes the analysis of a micelle system, created by a donor extended above a micelle surface, and a varying number of acceptors incorporated into the micelle surface (Aurell Wiström et al., 1996). There are two primary characteristics that distinguish this system from others: 1) random incorporation of acceptors into the micelle population and 2) the extension of the donor fluorophore above the micelle surface, creating a z-component to the transfer geometry. Using a function combining micelle geometry-dependent FRET and a Poisson distribution we have examined the ability of steady-state and excited-state lifetime fluorescence spectroscopy to resolve donor and acceptor placements on the micelle (Fig. 2 and Eq. 6).

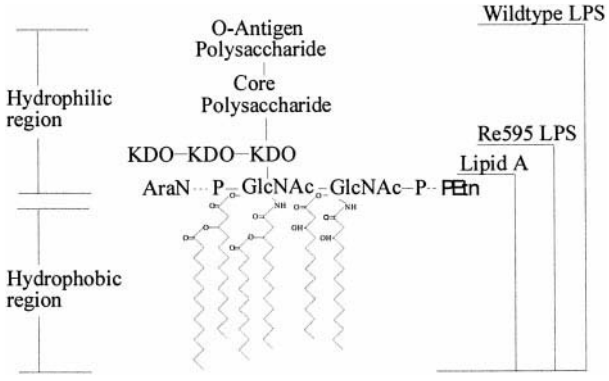

FIGURE 6 Typical structure of LPS (Shands and Chun, 1980; Labischinski et al., 1985; Raetz, 1990). GlcNAc, *N*-acetylglucosamine; P, phosphate; KDO, 2-keto-3-deoxyoctulosonic acid; PEtn, phosphoethanolamine; AraN, 4-amino-4-deoxy-L-arabinose. Also shown are the regions comprising lipid A, the Re mutant, and the wild-type LPS. Dashed lines represent nonstoichiometric additions or attachments currently in question.

Consequences of filling micelles with acceptors following a Poisson distribution

At low L, micelles without acceptors play an important role in the transfer observed (Fig. 1 and Eq. 6). Values of $L > 2$ insure that >90% of the micelles have acceptor.

Simulated steady-state data

Steady-state fluorescence data (see Fig. 3 and Table 1) created using Eqs. 18 and 19 show that there are character-

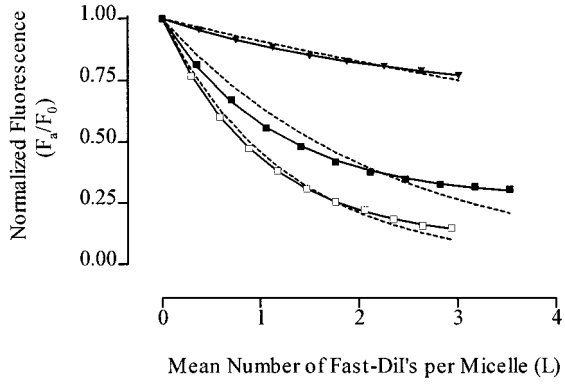

FIGURE 7 Fast-DiI quenching of 30 nM FITC-LPS solubilized in 100 μM SBP. ▼, *S. minnesota* wild type; ■, *S. ab. equi*; □, *S. minn.*, Re595. Dashed lines are single component fits to Re595, *S. minn.* and *S. ab. equi.* Single-component fits (*broken lines*) minimizing the sum of squares in Eq. 20 used Eq. 18. Two component fits (*solid lines*) used Eq. 19.

TABLE 3 Calculated FRET parameters for several strains of LPS-FITC solubilized in SBP

LPS type	D_1 (Å)#,‖	D_2 (Å)#,‖	A§	σ¶
Re595	16–36*			2.7×10^{-2}
	0	$>1.5\ R_0$	0.91	4.0×10^{-3}
Wild type	67–91*			1.4×10^{-2}
	34–51*	92–122*	0.23	2.4×10^{-3}
S. ab. equi	38–56*			5.6×10^{-2}
	11–25*	$>1.5\ R_0$	0.73	6.2×10^{-3}

D_1 and D_2, donor-to-micelle surface distances generated by Eqs. 18 and 19; A, scaling factor used in Eq. 19; σ, standard deviation between calculated and experimental data, created by using Eq. 20. The ranges in D are a result of the uncertainty of κ^2 as discussed in Materials and Methods.
*Steady-state fluorescence data from Fig. 7.

istic differences in transfer for donors extended at different distances (cases 1, 2, and 3). The differences are in the dependence on L and the highest level of transfer. A mixture of long and short lengths, case 4, can show a dependence similar to an intermediate length (case 3) but shows unique saturation behavior at high L.

Simulated excited-state lifetime data

Analysis of quenching efficiencies at low L values is enhanced by analysis using lifetime fluorescence spectroscopy. Evident in Fig. 4 is the large difference in phase and modulation data when donors at intermediate D (case 3) were compared with the case of mixed large and small D (case 4). The differences between the two cases increase with the increase in L, similarly to the steady-state data.

As there is a large difference in quenching efficiency across the micelle when the donor is located at $D \approx R_0$ ($0.50 \geq E \geq 0.06$), it can be argued that the data representing intermediate quenching can be better fit with a distribution of lifetimes rather than a discrete lifetime. With this in mind, the cases of intermediate donor extensions were also fit using a Gaussian distribution combined with a discrete lifetime (Gryczynski et al., 1989). Although these fits produced somewhat lower values of χ^2 at $L < 2$, a significant overall improvement was not seen (data not shown).

TABLE 4 Fluorescence lifetime measurements for FITC-LPS solubilized in SBP

FITC-LPS type	DiI/micelle	τ_1 (ns)	τ_2 (ns)	f_1	α_2/α_1	χ^2
S. Re595	0	3.9	0.80	0.83	1.01	0.1
	1	3.8	0.62	0.77	1.84	0.5
	2	3.7	0.58	0.75	2.17	0.7
S. ab. equi	0	3.9	0.98	0.87	0.61	0.4
	1	3.8	0.65	0.85	1.04	1.0
	2	3.7	0.49	0.83	1.56	0.7
S. minnesota	0	3.9	1.29	0.86	0.50	0.3
	1	3.8	1.12	0.87	0.51	0.3
	2	3.7	0.91	0.89	0.51	0.2

Fast-DiI concentration is at 0, 1, and 2 acceptors/micelle on average. f_1 (see Eq. 17), fractional intensity of the fluorophore population with a lifetime of τ_1; α_2/α_1, ratio of the concentrations of fluorophores with lifetimes τ_2 and τ_1; χ^2, reduced χ^2 a numerical value measuring the goodness-of-fit.

Dependence of resolution on the Förster distance (R_0)

Fig. 5 *A* demonstrates that the resolution of various donor placements above the micelle surface depends upon the value of R_0 and the diameter of the sphere. It is apparent that R_0 can be chosen to optimize resolution for a particular donor position or to discriminate one position from another. As the micelle radius increases relative to R_0, surface density (acceptors/R_0^2), rather than a Poisson distribution, becomes the appropriate measure of acceptor incorporation into the sphere population (Fung and Stryer, 1978; Estep and Thompson, 1979; Wolber and Hudson, 1979; Sklar et al., 1980). This is also illustrated in Fig. 8, where Fig. 8 *A* shows that as the ratio of r/R_0 increases, the quantum yield (q_a) becomes insensitive to the size of the micelle. For instance, it was found at a value of $r = 0.78\ R_0$, transfer in a planar surface, as described by Wolber and Hudson, 1978, is similar to transfer in the micellar system. As evident in Fig. 8, *B* and *C*, this loss of sensitivity can be traced to the Poisson distribution. As shown in Fig. 8 *B*, at larger values of r/R_0 the majority of micelles are filled at relatively low surface densities. In contrast, at lower r/R_0 values the majority of micelles are without acceptors even at surface densities greater than 0.5 acceptors per R_0^2. Slow filling of the micelles at small values of r/R_0 results from L, the intrinsic measure of acceptor incorporation, being relatively insensitive to acceptor density when the micelle radius is less than R_0 (see Fig. 8 *C*). Thus, at r/R_0 values less than unity, the Poisson distribution is required to estimate the number of spheres unfilled at acceptor surface densities traditionally used in FRET studies.

Molecular conformation in the detergent micelle

We have analyzed a LPS model (see Fig. 6) to test FRET on a micelle. In this model, LPS anchors into the micelle using lipophilic carbon chains. Additionally, the acceptor, Fast-DiI, is assumed to position with the photoactive region of the molecule at the surface of the micelle (see Fig. 2). The mutant and wild-type LPSs are different in mass, a direct result of a diversity in their oligosaccharide chain lengths, which varies their extension from the micelle surface (Aurell Wiström et al., 1996). The mutant strain Re595 lacks both core and *O*-antigen chains, placing donors near the surface of the micelle. LPS from *S. minn.* and *S. ab. equi* bacteria are heterogeneous in the lengths of the *O*-antigen oligosaccharide chain (Shands and Chun, 1980; Peterson and McGroarty, 1985). These heterogeneous chain lengths translate into heterogeneous D in the detergent micelle system. The persistence of native lifetime and the steady-state analysis require a fraction of donors at distances greater than $1.5\ R_0$, which are minimally quenched in the

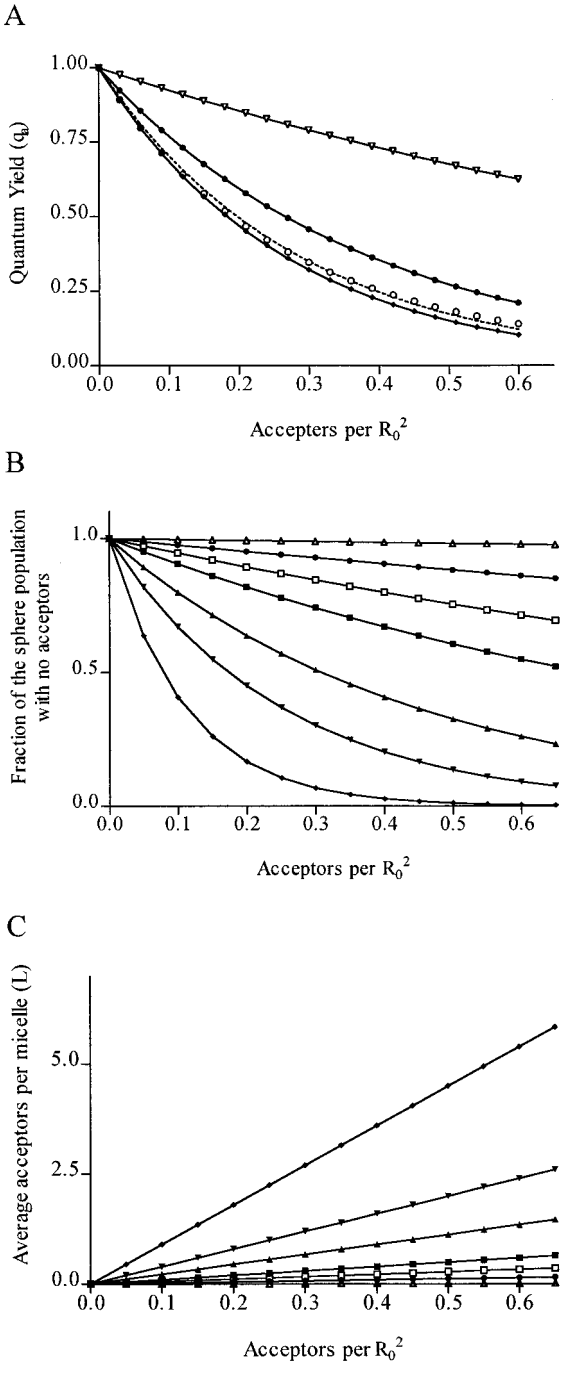

FIGURE 8 Effects of acceptor surface density and sphere size on components on the Poisson distribution and quantum yield. The effect of the Poisson distribution decreases with both increasing sphere size and increasing acceptor concentration. (*A*) Quantum yield as a function of acceptors per R_0^2. In this case the quantum yield was calculated using a modification of Eq. 18, where L was calculated in terms of acceptors per R_0^2. *B* and *C* show the effects that micelle size has on both the fraction of donors that do not participate in FRET (micelles without acceptors) and the average number of acceptors per micelle (L). $r/R_0 = 0.25$, ▽; 0.5, ●; 0.75, □; 1.0, ■; 1.5, ▲; 2.0, ▼; 3.0, ◆; ○, using Eq. 17 from Wolber and Hudson, 1979; and - - - a fit using Eq. 18 where $r = 0.78\ R_0$. (*B*) Fraction of the sphere population without acceptors ($P(0)$) as a function of surface density (acceptors/R_0^2). $P(0)$ is calculated from Eq. 6 at $k = 0$. (*C*) Average acceptors per micelle (L) as a function of surface density (acceptors/R_0^2).

presence of micelle-associated acceptors and a second population of donors that are near the surface. The analysis does not exclude the presence of donors at intermediate distances but rules them out as the major component. Thus, the model is sensitive to the presence of fluorophores extending well away from the micelle surface, which are minimally quenched, and fluorophores close to the surface, which are optimally quenched. The model is imprecise when the fluorophores are distributed heterogeneously at intermediate distances on the order of R_0. If fluorophores are located at three fixed (near, far, and intermediate) distances, the calculations suggest that they can be resolved if they have magnitudes of 20% or more.

The experiments themselves are subject to a number of experimental uncertainties, including donor and acceptor partitioning into the micelles, fluorophore clustering in the micelle, and the exact donor/micelle surface ratios. One general approach to handling these uncertainties is to compare the relative transfer efficiency between a lipid donor close to the surface and a donor placed at unknown distances on the molecule of interest. LPS has some characteristics that limit its utility as a model for developing micelle FRET. These include the anomalous short-lifetime behavior and the potential for heterogeneous overall length and placement of donors. An examination of Table 4 and Fig. 7 shows inconsistencies in steady-state and excited-state quenching, related to the anomalous short lifetime or arising from static quenching. Together, these issues relegate the lifetime analysis here to a qualitative and supporting role.

The micelle offers the possibility for analysis of donor-acceptor separation and molecular conformation of reconstituted lipophilic molecules. In addition, this approach has the potential to be used in the description of other characteristics of the system. For instance, if the transfer efficiency is known (for examples, all donors placed near the surface), the transfer is a simple measure of L, the number of acceptors per micelle. Alternatively, transfer in the micelle can be used as a measure of macromolecular assembly. Imagine the case where micelles are loaded with acceptor ($L \geq 3$), and a target molecule is associated with the micelle. Binding a ligand (conjugated to a fluorescent donor) to the target would result in transfer with the micelle-bound acceptors. Envisioning the micelle as a substitute for a cell membrane leads to the possibility of screening both direct and competitive molecular interactions. We envision measuring conformational changes in molecular assemblies such as those that might arise during cell signal transduction or adhesion.

REFERENCES

Abramowitz, M., and I. A. Stegun. 1965. Handbook of Mathematical Functions. National Bureau of Standards, Washington, D.C.

Aurell Wiström, C., G. M. Jones, P. S. Tobias, and L. A. Sklar. 1996. Fluorescence resonance energy transfer analysis of lipopolysaccharide in detergent micelles. *Biophys. J.* 70:988–997.

Badley, R. A., and F. W. J. Teale. 1971. Geometry and fluorescence of pepsin-substrate complexes. *J. Mol. Biol.* 58:567–578.

Castanho, M. A. R. B., and M. J. E. Prieto. 1992. Fluorescence study of the macrolide pentaene antibiotic filipin in aqueous solution and in a model system of membranes. *Eur. J. Biochem.* 207:125–134.

Chen, R. F., and J. R. Knutson. 1988. Mechanism of fluorescence concentration quenching of carboxyfluoroscein in liposomes: energy transfer to nonfluorescent dimers. *Anal. Biochem.* 172:61–77.

Cynkin, M. A., and G. Ashwell. 1960. Estimation of 3-deoxy sugars by means of the malonaldehyde-thiobarbituric acid reaction. *Nature.* 186: 155–156.

Dale, R. E., J. Eisinger, and W. E. Blumberg. 1979. The orientational freedom of molecular probes. *Biophys. J.* 26:161–194.

Doody, M. C., L. A. Sklar, H. J. Pownall, J. T. Sparrow, A. M. Gotto, Jr., and L. C. Smith. 1983. A simplified approach to resonance energy transfer in membranes, lipoproteins and spatially restricted systems. *Biophys. Chem.* 17:139–153.

Ediger, M. D., R. P. Domingue, and M. D. Fayer. 1983. Picosecond studies of excitation transport in a finite volume: the clustered transport system octadecyl rhodamine B in triton X-100 micelles. *J. Chem. Phys.* 80: 1246–1258.

Eis, P. S., and J. R. Lakowicz. 1993. Time-resolved energy transfer measurements of donor-acceptor distance distributions and intramolecular flexibility of a CCHH zinc finger peptide. *Biochemistry.* 32:7981–7993.

Estep, T. N., and T. E. Thompson. 1979. Energy transfer in lipid bilayers. *Biophys. J.* 26:195–208.

Fung, B. K-K., and L. Stryer. 1978. Surface density determinations in membranes by fluorescence energy transfer. *Biochemistry.* 17: 5241–5248.

Gennis, R. B., and C. R. Cantor. 1972. Use of nonspecific dye labeling for singlet energy-transfer measurements in complex systems: a simple model. *Biochemistry.* 11:2509–2517.

Gennis, L. S., R. B. Gennis, and C. R. Cantor. 1972. Singlet energy-transfer studies on associating protein systems: distance measurements on trypsin, α-chymotrypsin, and their protein inhibitors. *Biochemistry.* 11:2517–2524.

Gibson, G. A., and L. M. Loew. 1979. Application of Förster resonance energy transfer to interactions between cell or lipid vesicle surfaces. *Biochem. Biophys. Res. Commun.* 88:141–146.

Green, N. M. 1964. Avidin: quenching of fluorescence by dinitrophenyl groups. *Biochem. J.* 90:564–568.

Gryczynski, I., W. Wiczk, M. L. Johnson, and J. R. Lakowicz. 1989. Decay time distribution analysis of Y_t-base in benzene-methanol mixtures. *J. Photochem. B.* 4:159–170.

Haight, F. A. 1967. Generalizations of the Poisson distribution. *In* Handbook of the Poisson Distribution. John Wiley and Sons, New York. 30–66.

Herrmann, K. W. 1966. Micellar properties of some zwitterionic surfactants. *J. Colloid Interface Sci.* 22:352–3359.

Kaschke, M., O. Kittelmann, K. Vogler, and A. Graness. 1988. Picosecond absorption studies of intermolecular electronic energy transfer in micellar systems. I. Inhomogeneous spatial distribution and indirect donor-donor interaction. *J. Phys. Chem.* 92:5998–6003.

Kastowsky, M., T. Gutberlet, and H. Bradaczek. 1992. Molecular modeling of the three dimensional structure and conformational flexibility of bacterial lipopolysaccharide. *J. Bacteriol.* 174:4798–4806.

Kellerer, H., and A. Blumen. 1984. Anisotropic excitation transfer to acceptors randomly distributed on surfaces. *Biophys. J.* 46:1–8.

Labischinski, H., G. Barnickel, H. Bradaczek, D. Naumann, E. T. Rietschel, and P. Giesbrecht. 1985. High state of order of isolated bacterial lipopolysaccharide and its possible contribution to the permeation barrier property of the outer membrane. *J. Bacteriol.* 162:9–20.

Lakowicz, J. R. 1983. Principles of Fluorescence Spectroscopy. Plenum Press, New York.

Lakowicz, J. R., H. Cherek, I. Gryczynski, N. Joshi, and M. L. Johnson. 1987. Analysis of fluorescence decay kinetics measured in the frequency domain using distributions of decay times. *Biophys. Chem.* 28:35–50.

Maliwal, B. P., J. R. Lakowicz, G. Kupryszewski, and P. Rekowski. 1993. Fluorescence study of conformational flexibility of RNase s-peptide distance-distribution, end-to-end diffusion, and anisotropy decays. *Biochemistry.* 32:12337–12345.

Matyus, L. 1992. Fluorescence resonance energy transfer measurements on cell surfaces: a spectroscopic tool for determining protein interactions. *J. Photochem. B.* 12:323–337.

Peterson, A. A., and E. J. McGroarty. 1985. High-molecular-weight components in lipopolysaccharides of *S. typhimurium*, *S. minnesota*, and *Escherichia coli*. *J. Bacteriol.* 162:738–745.

Raetz, C. R. H. 1990. Biochemistry of endotoxins. *Annu. Rev. Biochem.* 59:129–170.

Sato, H., Y. Kusumoto, N. Nakasima, and K. Yoshihara. 1980. Picosecond study of energy transfer between rhodamine 6G and 3,3′-dimethythiacarbocyanineiodide in the perimicellar region: Förster mechanism with increased local concentration. *Chem. P. Lett.* 71:326–329.

Shahrokh, Z., A. S. Verkman, and S. B. Shohet. 1991. Distance between skeletal protein 4.1 and erythrocyte membrane bilayer measured by resonance energy transfer. *J. Biol. Chem.* 266:12082–12089.

Shands, J. W. Jr., and P. W. Chun. 1980. The dispersion of Gram-negative lipopolysaccharide by deoxycholate. *J. Biol. Chem.* 255:1221–1226.

Sklar, L. A., M. C. Doody, A. M. Gotto, Jr., and H. J. Pownall. 1980. Serum lipoprotein structure: resonance energy transfer localization of fluorescent lipid probes. *Biochemistry.* 19:1294–1301.

Skelly, R. R., P. Munkenbeck, and D. C. Morrison. 1979. Stimulation of T-independent antibody responses by hapten-lipopolysaccharides without repeating polymeric structure. *Infect. Immun.* 23:287–293.

Stryer, L. 1978. Fluorescence energy transfer as a spectroscopic ruler. *Annu. Rev. Biochem.* 47:819–846.

Szabo, G., Jr., P. S. Pine, J. L. Weaver, M. Kasari, and A. Aszalos. 1992. Epitope mapping by photobleaching fluorescence resonance energy transfer measurements using a laser scanning microscope system. *Biophys. J.* 61:661–670.

Wolber, P. K., and B. S. Hudson. 1979. An analytic solution to the Förster energy transfer problem in two dimensions. *Biophys. J.* 28:197–210.

Wu, P., and L. Brand. 1994. Resonance energy transfer: methods and applications. *Anal. Biochem.* 218:1–13.